Alma Mater Studiorum Università di Bologna
Archivio istituzionale della ricerca

Bidimensional H-Bond Network Promotes Structural Order and Electron Transport in BPyMPMs Molecular Semiconductor

(Article begins on next page)

02 May 2024

WILEY-VCH

Bidimensional H-Bond Network Promoters Structural Order and Electron Transport in BPyMPMs Molecular Semiconductor

Antonio De Nicola,* Andrea Correa, Andrea Giunchi, Luca Muccioli, Gabriele D'Avino, Junji Kido and Giuseppe Milano

Dr. Antonio De Nicola, Prof. G. Milano, Prof. J. Kido
Frontier Center for Organic Materials (FROM), Yamagata University,
4-3-16 Jonan, Yonezawa, Yamagata 992-8510, Japan
E-mail: adenicola@yz.yamagata-u.ac.jp

Prof. A. Correa
Dipartimento di Scienze Chimiche, Università di Napoli Federico II,
Complesso di Monte S. Angelo, 80126, Napoli, Italy

Prof. L. Muccioli, Dr. A. Giunchi
Dipartimento di Chimica Industriale "Toso Montanari", Università di Bologna,
40136 Bologna, Italy

Dr. G. D'Avino
Grenoble Alpes University, CNRS, Grenoble INP, Institut Néel,
25 rue des Martyrs, 38042 Grenoble, France

Prof. G. Milano
Dipartimento di Chimica e Biologia "Adolfo Zambelli", Università degli Studi di Salerno,
84084 Fisciano, Italy

The presence of a hydrogen bond (H-Bond) network has been proved to impact significantly the Organic Light Emitting Diode (OLED) devices efficiency by promoting molecular orientation and structural anisotropy in thin films. The design of specific compounds to control H-Bond network formation in an amorphous material, and hence to improve OLED performances, is needed. A successful example is given by the bi-pyridyl based family n-type of organic semiconductors named BPyMPM. The experimental evidences demonstrated a surprisingly higher electron mobility in thin film composed of B4PyMPM (B4), which is almost two order of magnitude higher than mobility measured for very similar member of the family, B2PyMPM (B2). We present a comprehensive computational study, where classical and ab-initio methods were combined, to investigate the 2D H-Bond network in B4 and B2 thin films. The results indicate that B4 forms a larger number of intermolecular C-H···N H-Bonds which

promote a higher orientational and positional order in B4 films, and superior electron transport properties.

1. Introduction

The OLED research field has constantly grown in the last 35 years: Scopus web archive counts roughly 12000 publications from 1994 to 2020, while the number of publications per year is still increasing.[1]

Nowadays OLEDs dominate the display market and show promise for a similar success in lighting applications in the near future, owing to the high brightness and the low power consumption they can offer. New generation OLEDs are produced by vapor-deposition (VP) of organic materials which form layers, wherein the molecular orientation is documented to be a key property capable to improve outcoupling and charge transport efficiency.[2]–[10]

The VP process allows producing smooth films with control over thickness on the nanometer length scale, by condensing molecules from the gas phase onto a temperature-controlled substrate.[11] As a disadvantage, that technique offers much less control over molecular orientation and crystallinity, which are governed by a complex interplay between kinetic and thermodynamic effects, often substrate-dependent.[12],[13] A viable strategy to maximize the thermodynamic thrust is to design molecules with specific shapes and functional groups that promote highly directional supramolecular interactions.

In this context, Prof. Yokoyama and co-workers demonstrated the general relationship between the structural anisotropy of a given molecule and its orientational order and preferred alignment direction in a thin solid film.[14],[15] In another series of studies, intermolecular C-H···N H-Bonds were exploited for driving the supramolecular assembling, by designing molecules containing multiple pyridine rings[6] properly arranged in order to maximize intermolecular interactions that promote long-range structural order.[5–7]

This strategy was showed to be successful and several molecules were demonstrated to form flat surfaces and regular stacking through self-assembly.[5]–[7],[16] Besides, the presence of a bidimensional H-Bond network promotes anisotropic optical properties, like the refractive index and extinction coefficient k, and a non-negligible electron mobility.[6] Remarkably, a difference of about two orders of magnitude in the electron mobility, from time-of-flight measurements, was found between vacuum deposited films composed of B4 ($\sim 10^{-4} cm^2 V^{-1} s^{-1}$) and B2 ($\sim 10^{-6} cm^2 V^{-1} s^{-1}$) respectively,[6] whose chemical structure is reported in Figure 1.

The understanding of the driving forces regulating molecular orientation is mandatory to optimize material properties, such as charge transport, and to design processes and/or compounds to improve device efficiency. In this matter, the molecular dynamics (MD) at atomic resolution is a powerful computational method able to rationalize the microscopic origin of the molecular preferred orientation,[17]–[26] and several studies have been reported to successfully study interfacial properties and molecular arrangement of OLED materials.[7,18,20,27] For a general description of the challenges and the strategies currently used in the computational modelling of OLED materials, we refer the interested reader to a recent perspective[19] and the references therein.

In the present study, all-atom MD simulations are employed to investigate the molecular orientation of B4 and B2 in thin films as final aim. The role of the H-Bond network and its consequences on the molecular geometries and electrical properties are investigated with Density Functional Theory (DFT). The paper is organized as follows: in the Methods and Models section the atomistic model description, force-field optimization, simulation protocol, electronic structure calculations, and computational details, are reported. The structural and charge properties calculated from MD simulations are discussed and compared with experiments in the Results section, while the main results are summarized in the Conclusion section.
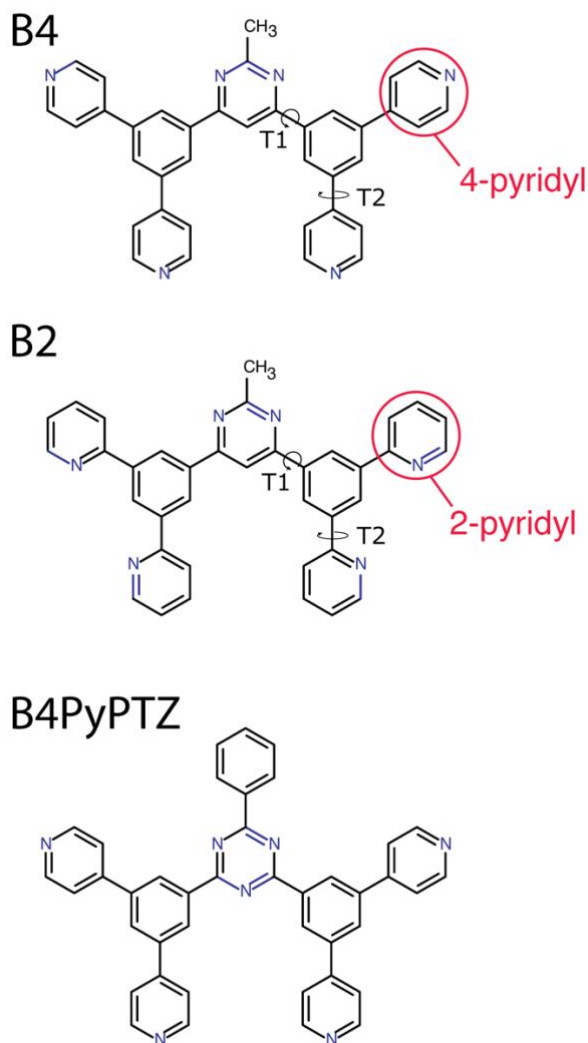
Figure 1. Chemical structure of B4, B2, and B4PyPTZ molecules. The different position of nitrogen atoms in the 4- and 2-pyridyl rings in B4 and B2 molecules are indicated. The dihedral angles φ_{T1} and φ_{T2} responsible for the conformation of the molecules are also indicated.

2. Methods and Models
2.1. Molecular Dynamics Simulations

All the atomistic simulations reported in the paper were performed by using the GROMACS simulation package.[27],[28] A time step of 2 fs has been employed for all simulations. The temperature, in both NVT and NPT ensembles, has been held constant at 298 K by using a stochastic velocity rescaling algorithm[29] with a characteristic coupling time $\tau_T = 0.02$ ps; moreover, in the NPT ensemble the pressure has been kept constant at 1 atm by using the Berendsen barostat[30] (pressure coupling time $\tau_P = 0.2$ ps, compressibility of 1×10^{-5} bar^{-1}, anisotropic scaling of box sides with the same τ_P value for x, y, z directions). All the bonds

involving hydrogen atoms have been constrained using the LINCS algorithm.[31] Lennard-Jones interactions were calculated by using a cut-off distance of 1.4 nm, while electrostatic interactions have been treated with the Particle Mesh Ewald algorithm[32] with a grid spacing of 0.1 nm. System compositions and total simulation times are listed in Table 1.

Table 1. Characteristics of the simulated systems.

System	No. Molecules	Molecule Type	Ensemble	Average Box Length [x,y,z] (nm)	Time (ns)
Bulk	128	B4PyPTZ	NPT	5.382 ± 0.1, 3.514 ± 0.08, 5.443 ± 0.1	100
Bulk	128	B4	NPT	4.698 ± 0.1, 3.596 ± 0.1, 5.701 ± 0.12	100
Bulk	128	B2	NPT	5.102 ± 0.1, 3.587 ± 0.1, 5.567 ± 0.17	100
Film	128	B4	NVT	4.751, 3.627, 25.706	350
Film	128	B2	NVT	5.069, 3.561, 25.566	350

2.2 Atomistic Model

We adopted the atomistic OPLS force field (FF), developed by Jorgensen in 1996,[34] except for soft aryl-aryl torsions. These torsions and their energy barriers are fundamental in determining the molecular shape and must be described accurately for a correct modeling.[35] For instance, a recent extension of the OPLS-AA has been optimized to improve the description of inter-ring torsions [36] for molecules containing biaryl groups. Following these guidelines, we made a reparameterization of the Fourier coefficients used in the Fourier series sum describing the torsional energy profile (see eq. S4 of Supporting Information). In particular, the torsional energy profiles for φ_{T1} and φ_{T2} dihedral angles were calculated (see Figure 1 for their definition). The geometries of B4 and B2 molecules have been optimized at different fixed aryl-aryl angles (with steps of 10º), at PBE0/6-311G** level,[36]–[38] using Gaussian09.[33] By fitting the torsional energy profile from DFT calculations of φ_{T1} and φ_{T2} dihedral angles, Fourier coefficients are obtained. The comparison between torsional energy profiles at DFT and FF level is reported in the section 1 of Supporting Information together with the full list of FF parameters and the functional forms of bonded and non-bonded interactions.

2.3 Sample Preparation

The thin films of B4 or B2 compounds, prepared via vacuum deposition, possess to some extent an ordered structure, presumably due to a columnar arrangement favored by the presence of a bidimensional H-Bond network.[6] Since the structural information in the solid state of B4 and B2 is not available, we built thin films initial configurations starting from the experimental crystal structure of a molecule, B4PyPTZ (see Figure 1), having optical properties and chemical structure similar to B4 and B2. The crystallographic unit cell of B4PyPTZ,[5] containing 16 molecules, has been replicated 2 × 2 × 2 times along *a, b, c* directions to build a supercell composed of 128 molecules. The B4PyPTZ crystalline structure is characterized by molecules stacked in columns in which the peculiar position of pyridine nitrogen atoms maximizes the probability to form of intermolecular H-Bonds with adjacent columns, creating a bidimensional H-Bond network.[5]

The stability of B4PyPTZ sample has been checked performing a MD simulation in the NPT ensemble employing the OPLS-AA force field with the tuned torsional potential for φ_{T1}, φ_{T2} angles. The equilibrium mass density obtained from the MD simulation (1278 kg/m^3 ± 5 kg m^{-3}) slightly underestimates the experimental value[5] of about 3%, however, the deviation from the experimental value is similar to those observed for the majority of organic molecules in solid phase (2-4%) modelled by using OPLS force field.[34]–[38] Besides, the lattice constants (*a, b, c*) of crystalline structure are reproduced within an error of +1.9%. The time behavior of the mass density and the X-Ray pattern calculated on the equilibrium structure are reported in Figures S5, S6.

The equilibrium structure of the B4PyPTZ supercell was used as initial coordinate set to build B4 and B2 systems. The description of the procedure employed to build systems and further details about it are reported in the Supporting Information. NPT simulations revealed a difference in the equilibrium mass density among the two bulk systems, even if the only difference between the two molecules lies in the position of nitrogen atoms in the pyridine rings

(Figure 1). Starting from initial configurations, at the same density for both molecules, the bulk of B4 reaches a slightly higher equilibrium value (1197 ± 5 kg m^{-3}) than B2 (1176 ± 5 kg m^{-3}) revealing a more efficient packing (Figure S8).

2.4 Electronic Structure Calculations

Most organic semiconductors with mobilities below ~1 cm^2/Vs are characterized by thermally activated hopping-like transport. The most popular, semiclassical rate equation for charge hopping is due to Marcus[39] (Equation 1), stating a proportionality between the rate between two molecules i and j and the square of the intermolecular electronic coupling J_{ij}, and an Arrhenius-like exponential dependence with activation barrier $(\Delta G_{ij} + \lambda)^2/4\lambda$:

$$k_{ij} = \frac{2\pi}{\hbar} \frac{J_{ij}^2}{\sqrt{4\pi\lambda k_B T}} \exp\left[-\frac{(\Delta G_{ij}+\lambda)^2}{4\lambda k_B T}\right] \tag{1}$$

Where $\lambda = \lambda_i + \lambda_s$ is the total reorganization energy, quantifying the dynamic energetic fluctuations and including both the internal (λ_i) and environmental contribution (λ_s); ΔG_{ij} is the difference between the molecular site energies (averaged over dynamic fluctuations) and eventually including the effect of an applied electric field. For electron transport, the site energies correspond to the electron affinity with reversed sign, i.e. $\Delta G_{ij} = -EA_j + EA_i$.

The site energy of a given molecule includes an intramolecular and an environmental component:[40]

$$EA = EA_{gas} - \Delta \tag{2}$$

The term EA_{gas} corresponds to the electron affinity of the isolated molecule, and we approximate it with the LUMO energy, E_{LUMO}. The environmental component Δ is instead obtained with classical microelectrostatic (ME) calculations using MESCal code,[41] in which molecules interact through forces between atomic permanent charges and atomic induced dipoles, the latter requiring a self-consistent treatment of mutual interactions. The environmental contribution to site energies can be further partitioned into an electrostatic (Δ_E) and an induction (Δ_I) term, $\Delta = \Delta_E + \Delta_I$. In particular, Δ_E corresponds to the energy to charge a molecule in the electrostatic potential of the permanent and induced multipoles of the surrounding molecules in the neutral sample, while Δ_I accounts for the dielectric screening of the added charge by the polarizable medium.[42] The induction term Δ_I affects the absolute values of the energy levels, typically increasing the EA by ~ 1 eV, but it is essentially isotropic and then contributes only marginally to the spread of the transport levels.[40] Then, this term is here disregarded, since our primary interest is the estimation of energetic disorder.

Our samples are characterized by the presence of structural disorder which may strongly affect the energetics of localized charge carriers (see e.g. ref. [43] for a discussion of different effects in play). In fact, each molecule experiences a different electrostatic environment, and this leads to a broad distribution of charge transport levels. These distributions often feature an approximately Gaussian shape, whose standard deviation σ is taken as a measure of the energetic disorder. The broadening of transport levels has been estimated upon sampling the EA over all the molecules, and for 11 MD trajectory snapshots (configurations extracted every 10 ns of the last 100 ns of production runs), resulting in time series of molecular site energies $x_m(t_i)$. This sampling allows us also to partition the total energetic disorder, σ, in its static (or positional) and dynamic components.[40] To such an aim, we define the average $\bar{x}_m$ and the variance σ_m^2 of the energy of molecule m over time. The static disorder corresponds to the variance of molecular time-averaged site energies, $\sigma_{static} = \sqrt{\langle(\bar{x}_m - \langle\bar{x}_m\rangle)^2\rangle}$, where angle

brackets indicate the average over different molecules. The dynamic component quantifies the time fluctuations of molecular site energies, i.e. $\sigma_{dynamic} = \sqrt{\sigma^2 - \sigma_{static}^2} = \sqrt{\langle(\bar{x}_m - \langle\bar{x}_m\rangle)^2\rangle}$.

For the parameterization of the ME method, molecular polarizability and ESP charges for B2 and B4 neutral molecules and anions have been obtained at the equilibrium geometry by PBE0/cc-pVTZ DFT calculations using Gaussian16.[44] The simulated samples were treated as thin films, applying periodic boundary conditions in two dimensions (x, y) and constructing supercells of the original samples. We have verified that a cut-off of 44 nm (~ 8 times the average thickness of the samples) ensures a proper convergence of electrostatic interactions, i.e. within 50 meV for absolute energies and 5 meV for energy differences between sites. Electronic couplings were calculated for every pair of molecules ("dimers", having at least two atoms at distance lower than 7 Å) in a single configuration of the B2 and B4 samples. Calculations were carried out with the ORCA code[45], at DFT level B3LYP/6-31G(d) using the dimer projection method.[46] The intermolecular reorganization energies λ_i for B2 and B4 were calculated using the four-point method[47] via PBE0/cc-pVTZ calculations, and amount to 0.3 eV for B2 and 0.32 for B4, respectively. These values are considerably larger than the one of the prototypical n-type organic semiconductor C60 fullerene.[48],[49]

3. Results

3.1 B4 and B2 Thin Films

Since the experimental fabrication of B4 and B2 films is made by vacuum deposition, to mimic as much as possible experimental conditions MD simulations of the bulk/vacuum interface have been performed. The intent is to include the effect of the vacuum/film interface affecting molecular geometries and structural properties. To this aim, four independent configurations of B2 and B4 have been extracted from MD trajectories of bulk phase (a configuration every 20 ns of the last 80 ns of each trajectory) and used as a starting coordinate set to simulate vacuum/bulk interface systems. The vacuum interface has been built by increasing the box side (*z*) by 20 nm. Then, MD simulations in NVT ensemble have been performed for each independent

configuration. Representative snapshots of equilibrium configurations of B2 and B4 systems are reported in Figure 2.

The visual inspection of equilibrium configurations reveals a well-defined columnar structure for the B4 system (left side of Figure 2). Instead, B2 molecules are much more disorderly stacked on each other, and many of them appear tilted with the respect to the normal direction (z) of the bulk/vacuum interface (right side of Figure 2). A more quantitative indication is gained by computing the X-Ray powder pattern and the radial distribution function (g(r)).

As can be seen from panel A in Figure 3, both X-Ray traces show a peak at q~ 1.53 Å^{-1}, corresponding to molecular π-stacking distance.
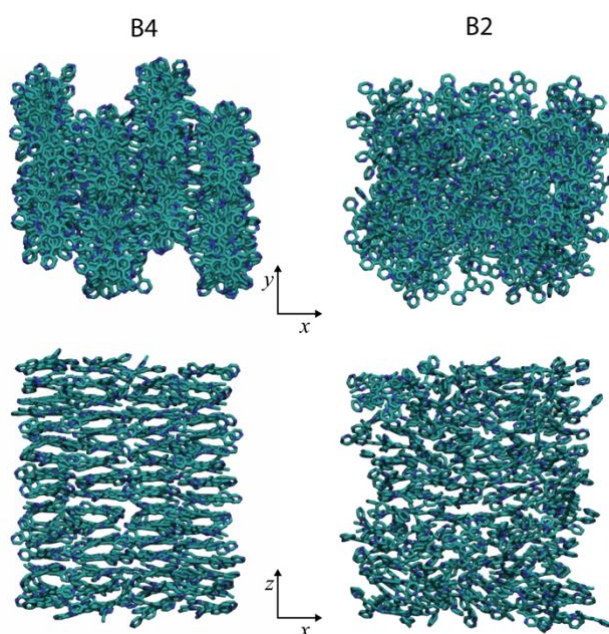
Figure 2. Snapshots representative of the equilibrium configuration of B4 and B2 systems. Nitrogen atoms are represented in deep blue and carbons in cyan. The hydrogen atoms are omitted for clarity. The vacuum/bulk interface is perpendicular to z direction.

The B4 profile shows a sharp peak at this position, which is comparable with the experimental spacing of ∼ 4 Å measured on a thin film of B4 material.[6] The comparison with the broader peak found for B2 indicates a decrease of positional order along the stacking direction for the latter system. The difference in the positional order between B2 and B4 systems is confirmed by the g(r) displayed in Figure 3B.
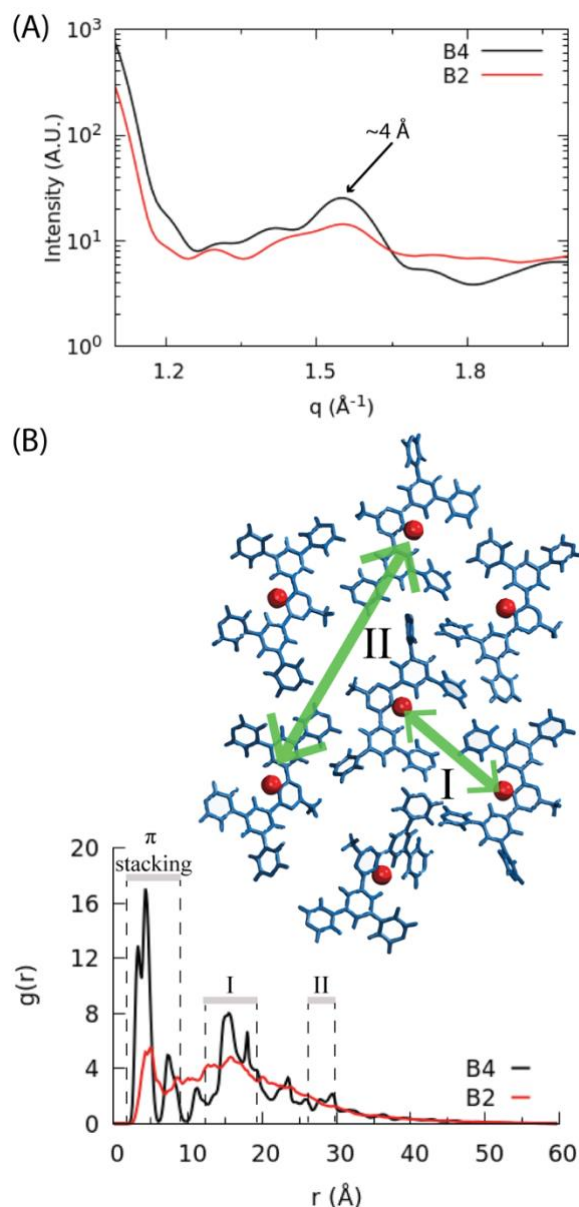
Figure 3. (A) X-Ray powder pattern is calculated using CuK_α radiation ($\lambda = 1.5418$ Å) as in the experiments.[6] Using the last 80 ns of trajectories, structure factor patterns for B4 (black) and B2 (red) were calculated by using the ISAACS package.[50] (B) Radial distribution functions g(r) calculated for the core hydrogens. Explicit assignment of the main peaks is reported in the plot. A snapshot of B4 system, counting seven molecules belonging to adjacent columns is reported to outline the hexagonal packing.

These functions have been computed by considering only the hydrogen atom belonging to the central pyrimidine ring; those atoms are shown as red spheres in the snapshot of Figure 3B. Due to its peculiar position, the pyrimidine hydrogen is a convenient choice to characterize structural properties at molecular (π-stacking) and bulk scales (hexagonal packing in case of B4). As can

be seen from the comparison between B2 and B4 curves, it is clear that B4 has much higher positional order, in particular in the region of π-stacking (∼ 3-5 Å) which is fundamental for promoting electron transport, with peaks about three times more intense than for B2. At larger distances, the B4 g(r) shows two main peaks, region I at ∼ 1.5 nm and region II at ∼ 2.8 nm, which represent the characteristic interplanar distances of the nearly hexagonal packing. Instead, B2 shows a featureless broad halo in the same region, which indicates lower structuration. Additional snapshots highlighting the hexagonal packing are reported in Figure S12. Since structural order and molecular orientation are correlated, a high positional order of B4 structure should correspond to a high orientational order, too. The regularity in molecular orientation can be computed using the orientational order parameter (P_2), which is defined as:

$$\langle P_2 \rangle = \frac{3\langle cos^2\theta \rangle - 1}{2} \tag{4}$$

where θ is the angle between an arbitrary molecular axis m, defined in Figure 4A, and a reference direction z. The angle brackets indicate the ensemble average. If we choose the molecular axis in the pyrimidine plane as in reference,[6] when every molecular axis is oriented parallel to the z vector (the normal to the surface), and hence in a perfect edge-on configuration, P_2 is equal to 1, while for an isotropic distribution of orientations P_2 equals to 0 and for a perfect face-on distribution, P_2 is equal to -0.5. In Figure 4B, computed and experimental P_2 are compared: while for B2 the orientational order is slightly overestimated with respect to the measured value, the calculated values show the same trend of the experimental data, with B4 being more ordered that B2. More in detail, we observe that B4 molecules have a more pronounced "face-on" orientation than B2. The tendency to form well-ordered columnar stacks is beneficial for key properties such as charge transport and efficiency in OLEDs devices, as reported by Kido and co-workers.[4]–[7],[51]
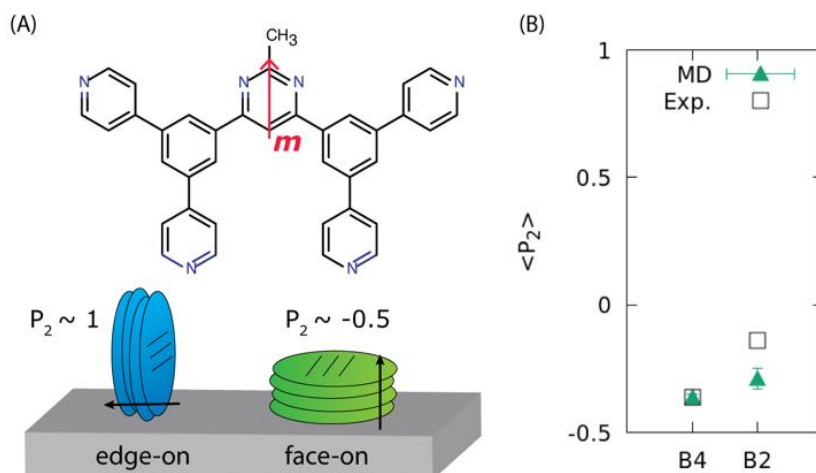
Figure 4. (A) scheme showing the definition of molecular axis m (red arrow) and face-on, edge-on orientation on a substrate. (B) $\langle P_2 \rangle$ calculated from MD simulations (solid triangles) and from experiments[6] (open squares).

3.2 Hydrogen Bonds

The higher solubility of B4 in chloroform with a small amount of methanol is an evident experimental proof of the strongest tendency of B4 to form H-Bonds with respect B2.[6] In addition, the presence of a strong bidimensional H-Bond network was also demonstrated by scanning tunneling microscopy (STM) experiments carried out at the interface between a solution of B4 and a graphite surface.[52]–[56]

To detect H-Bond features, simulation trajectories have been analyzed in detail. The B2 and B4 molecular structures display several possible (weak) H-Bond acceptor (A) and donor (D) sites (definitions in Figure 5A). During the simulation, a hydrogen bond is counted when two geometrical conditions are simultaneously satisfied:[57] First, the distance between A and D must be shorter or equal to r_C cut-off distance of 0.3 nm; second, the angle $\theta_{(A-H-D)}$ must be larger than $\theta_{cut-off} = 120º$. We have tested different cut-off distances and cut-off angles in the H-Bond counting to verify the correct applicability of the used values proposed in reference.[57] Additional analyses are reported in the Supporting Information.

In agreement with the experimental evidences,[6],[52]–[56] we have found a higher average number of H-Bonds/molecule (~ 2.5) for B4 with respect to B2 (1.5), as shown in the histogram in

Figure 5B. According to a geometrical criterion based on the π-stacking distance (~ 4 Å), hydrogen bonds were also labelled as in-plane or out-of-plane. If the D-A distance along the normal direction of bulk/vacuum interface z between D and A is longer than 4 Å, the H-Bond is counted as out-of-plane; for shorter distances is counted as in-plane, or in other words the bond is roughly coplanar with the molecular planes. The fraction of in-plane bonds is reported in Figure 5, panel C, alongside the intra molecular H-Bond fraction in panel D. In case of B4, most H-Bonds are formed between molecules lying a same plane (~ 0.87), instead, a lower fraction (~ 0.58) is found for B2. Furthermore, B4 molecules do not form, in practice, intramolecular H-Bonds, while B2 has a noticeable amount of them (nearly 13%, Figure 5D). These results, in addition to previous structural results (including order parameter, X-Ray pattern, g(r) and mass density) confirm the interpretation of the 3D assembly given by Kido and co-workers[6] and also discussed in the interpretation of B4 two dimensional structures.[52]–[56]

In addition, B4 pyridine nitrogen atoms are positioned at the very edge of the molecule, and then favoring in-plane connections between pairs of coplanar molecules via intermolecular H-Bonds, and the formation of a bidimensional network. In fact, ~ 84% of that hydrogen atoms of B4 molecule are involved in the H-Bond formation (section 2.3.3 of the Supporting Information). The ortho position of nitrogen atoms in pyridine rings in B2, instead, implies a rotation of those rings to maximize the number of intermolecular H-Bonds (~ 70% of external hydrogen atoms are involved in the H-Bond formation, Table S7 of Supporting Information). However, even if a 2D H-Bond is formed, such a rotation of reduces the planarity and, consequently, the packing ability of B2. This is clearly reflected by the lower mass density reached by B2 bulk, reduced structural order and lower number of H-Bonds per molecule with respect to B4. In addition to those evidences, the distributions of φ_{T1} and φ_{T2} dihedral angles suggest a slightly higher planarity for B4 (Figure S13 of Supporting Information).
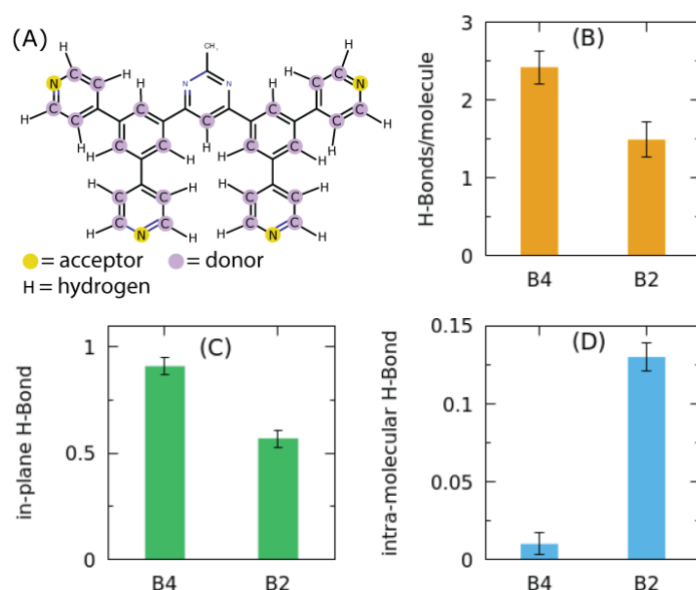
Figure 5. (A) definition of hydrogen bond acceptor and donor sites for B4. (B) average number of H-Bonds/molecule. (C) In-plane H-Bond fraction, and (D) intra molecular H-Bond fraction. Data has been computed on the last 35 ns of MD trajectories.

3.3 Electron Transfer Parameters

As already mentioned, Kido and co-authors measured the electron mobility of B2 and B4 with the time of flight technique, obtaining at room temperature values of the order of 10^{-6} and 10^{-4} cm^{2}V^{-1}s^{-1}, respectively.[6] In this section, exploiting the atomic resolution of the system morphologies provided by MD simulations, we aim at establishing a link between structural and electronic properties, and analyze the factors that contribute to the large offset between B2 and B4 mobility.

We begin the comparison of the charge transport properties of the two systems by inspecting the distributions of electron affinities, i.e. the density of states available to charge carriers. The histograms in Figure 6 clearly show two main differences: first, B4 has an electron affinity larger than B2, which is a positive characteristics because it improves the air stability of the semiconductor[58] and facilitates a possible doping by electron donating impurities. Moreover, the distribution of electron affinity for B4 is narrower than the one for B2. Again, this goes in favor of superior electron transport in the B4 system, since the distribution standard deviation

σ quantifies the energetic disorder, which in turn is one of the main limiting factors for charge mobility.[43]
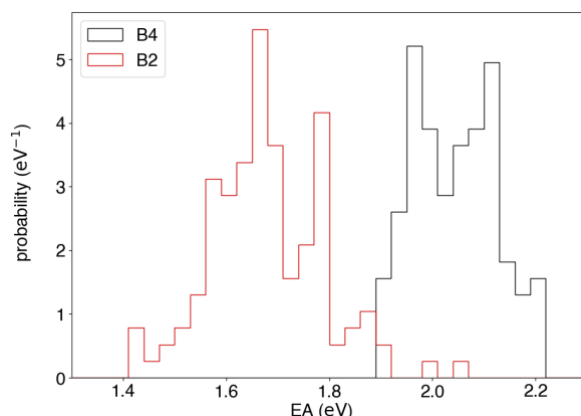
Figure 6. Distribution of electron affinities for B4 and B2, averaged on eleven MD configurations. Individual values were obtained as $EA = -(E_{LUMO} + \Delta_E)$ by DFT and microelectrostatic calculations.

We note that the calculated static disorder of EA is larger for B2, and qualitatively in line with the experimental values (0.091 and 0.076 eV for B2 and B4, respectively[6]), which were obtained by fitting mobility dependence on electric field and temperature with an empirical but well established equation for amorphous semiconductors[59]. This observation reflects the higher structural order present in B4 samples. The amount of dynamic disorder is instead rather similar for the two systems, yet again slightly larger for B2: these room-temperature energetic fluctuations correspond to a reorganization energy $\lambda = \sigma^2_{dynamic}/k_B T$ about 0.12 eV higher for B2. From Table 2 it can be further seen that the difference in energetic disorder between the two systems, both for the static and dynamic component, is sourced from the environmental electrostatic contribution Δ_E, while the fluctuations of the LUMO energies are quite similar, albeit again a bit larger for B2.

To explain the higher disorder of the energy levels in B2 and its chiefly dynamic nature, let us consider the four terminal pyridine units: any thermally activated rotation about the pyridine-phenyl bond (φ_{T2} torsion in Figure 1) marginally affects the electrostatic layout of B4, where the local dipole associated with the pyridine nitrogen is coaxial with the bond. On the other

16

hand, pyridine rotations can produce a rather large variation of charge distribution for B2, where the dipole is off-axis. This makes that, for B2, a given amount of dynamic conformational disorder translates in more important variations of the electrostatic landscape felt by charge carriers. The argument is strengthened by the DFT calculation of the gas phase molecular dipoles along the trajectories, that yields larger values and fluctuations for B2: 2.9 ± 1.3 D versus 0.8 ± 0.3 D for B4.

Table 2. Averages of intramolecular (E_{LUMO}), intermolecular (Δ_E), and total electron affinities ($EA = -E_{\text{LUMO}} - \Delta_E$), and corresponding standard deviations separated in static and dynamic contributions σ_{static} and $\sigma_{dynamic}$. Average Energies are in eV, standard deviations in meV.

B2	average	σ_{total}	σ_{static}	$\sigma_{dynamic}$
E_{LUMO}	-1.681	97	50	83
Δ_E	0.000	181	124	132
EA	1.681	183	111	145
B4	average	σ_{total}	σ_{static}	$\sigma_{dynamic}$
E_{LUMO}	-2.201	81	30	75
Δ_E	0.156	129	67	110
EA	2.046	156	81	134

We now focus our attention on the magnitude and fluctuations of intermolecular electron-transfer couplings J, representing the pre-exponential factor in Equation1, and on their relationship with the structural organization in the simulated samples. Figure 7A compares the magnitude and directionality of these couplings between the two materials, reporting the absolute value of J, computed for molecular pairs in our MD samples, against r_z/r (gray dots), being r the module of the intermolecular distance and r_z its z-axis component. Charge transfer couplings are highly anisotropic in both systems (see also Figure S18), attaining appreciable values only when the intermolecular vector is parallel to the stacking direction ($r_z/r > 0.6$). As better appreciated by observing the average values of $|J|$ over r_z/r intervals (red squares), the magnitude of the couplings is significantly larger in B4 than in B2, and this difference determines a superior electronic connectivity with respect to B2. This quantity, shown in Figure

7B, corresponds to number of neighbors that, on average, is connected to each molecule by a coupling exceeding a given value of $|J|$. The two systems approach in a very different way the connectivity of 2 characteristic of an ideal 1D semiconductor, with e.g. B4 attaining the value of 1.5 with couplings of 41 meV, and B2 only for $|J| = 12$ meV.

The superior charge transfer properties of B4 as compared to B2 are completely unexpected at the molecular level, given the similar structure and the nearly identical LUMO orbitals (see inset Figure 7A) of the two molecules.[6] We infer that the difference between the two materials may be due to the better supramolecular packing of B4 discussed above. To prove this hypothesis with an "alchemical" experiment, impossible to perform with real systems, we have computed the intermolecular couplings for a fictitious B4 phase, obtained from the atomic coordinates of the B2 sample by switching the positions of the N atom and one CH group in the peripheral pyridine rings. Figure 7C, compares the couplings of this hypothetical sample, labelled "B4 < B2", with the original B2 ones. This plot reveals a nearly perfect correlation between the two data sets (Pearson coefficient R=0.994), demonstrating that the difference between the charge transport properties of the two materials does not arise from the chemical structure. It has instead to be ascribed to the better molecular organization in B4, in turn resulting from the presence of a two-dimensional H-Bond network.
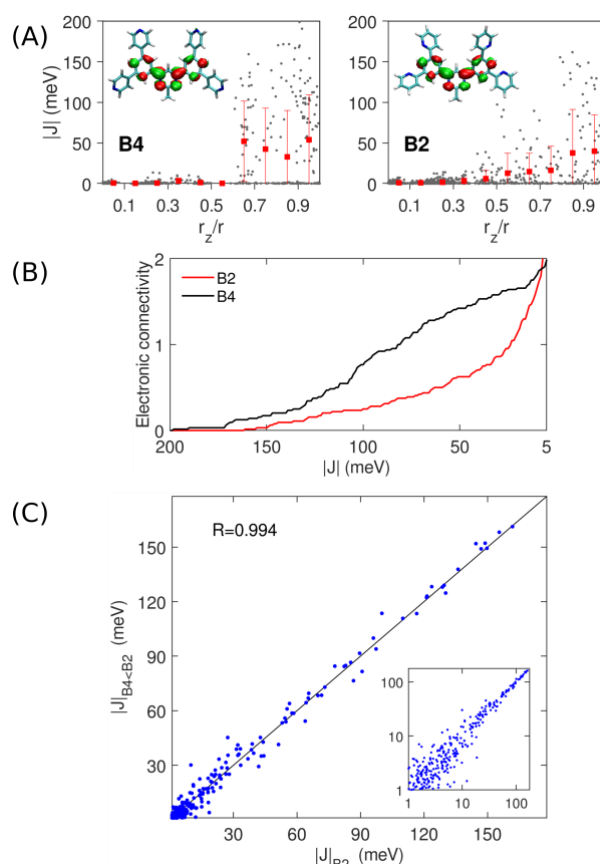
Figure 7. (A) Electron-transfer couplings as a function of the normalized projection of the intermolecular vector distance $\mathbf{r}$ along the stacking axis z. Gray dots show the couplings computed for molecular pairs extracted from the MD sample, red squared (error bars) show the mean value (standard deviation) over intervals of r_z/r. LUMO orbitals of B4 and B2 are shown as insets. (B) Electronic connectivity, i.e. average number of neighbors per molecule having an electronic coupling larger than the abscissa value. (C) Correlation between the couplings of B2 and those of a fictitious B4 sample obtained modifying the atomistic morphologies of B2 (see text). The quadrant bisector (black line) is shown as a guide for the eye. The same plot in a log-log scale in shown as an inset.

4. Conclusions

Combining DFT calculations and MD all-atom simulations we investigated the role of intermolecular hydrogen bonds in the molecular orientation, stacking and electron mobility of thin films composed of pyridine-based molecules B2 and B4.

The only difference between the B4 and B2 chemical structure lies in the position of nitrogen atoms in the four outer pyridine rings, which is surprisingly sufficient for causing a huge difference in the optical and electron transport properties, as experimentally proved. We found that B4 has a higher capability to connect with adjacent molecules, by forming intermolecular

hydrogen bonds, compared with B2 (2.5 vs 1.5 bonds per molecule). The stronger 2D H-Bond network formed for B4 is enough to stabilize a supramolecular organization in which molecules form ordered layers and columns.

The calculation of essential electron transport parameters, such as reorganization energies, site energies, and electronic couplings revealed that the microscopic origin of the higher electron mobility of B4 with respect to B2 has its roots in lower reorganization energy and electrostatic disorder and, more importantly, in the superior morphology promoted by the hydrogen bond network.

On a general vein, our findings disclose how intermolecular hydrogen bond interactions promote structural order in molecular thin films, ultimately improving their electron transport properties. The engineering of these weak interactions offers viable opportunities for the rational design of new materials with improved performances in OLED applications.

Notes

B4 = B4PyMPM = (4,6-bis(3,5-di(pyridine-4-yl)phenyl)-2-methylpyrimidine

B2 = B2PyMPM = (4,6-bis(3,5-di(pyridine-2-yl)phenyl)-2-methylpyrimidine

B4PyPTZ = 2,4- bis(3,5-di-4-pyridinylphenyl)-6-phenyl-1,3,5-triazine

Supporting Information
Supporting Information is available from the Wiley Online Library or from the author.

References

[1] scopus.com https://www.scopus.com/ (accessed May 19, 2020).

[2] Marcato T., Shih C. J. *Helv. Chim. Acta* **2019**, *102* (5). https://doi.org/10.1002/hlca.201900048.

[3] Boehm B. J., Nguyen H. T. L., Huang D. M. *J. Phys. Condens. Matter* **2019**, *31* (42). https://doi.org/10.1088/1361-648X/ab2ac2.

[4] Ohisa S., Pu Y.-J., Yamada N. L., Matsuba G., Kido J. *ACS Appl. Mater. Interfaces* **2015**, *7* (37), 20779–20785. https://doi.org/10.1021/acsami.5b05818.

[5] Watanabe Y., Sasabe H., Yokoyama D., Beppu T., Katagiri H., Pu Y. J., Kido J. *Adv. Opt. Mater.* **2015**, *3* (6), 769–773. https://doi.org/10.1002/adom.201400532.

[6] Yokoyama D., Sasabe H., Furukawa Y., Adachi C., Kido J. *Adv. Funct. Mater.* **2011**, *21* (8), 1375–1382. https://doi.org/10.1002/adfm.201001919.

[7] Watanabe Y., Yokoyama D., Koganezawa T., Katagiri H., Ito T., Ohisa S., Chiba T., Sasabe H., Kido J. *Adv. Mater.* **2019**, *31* (18), 1–8. https://doi.org/10.1002/adma.201808300.

[8] Duhm S., Heimel G., Salzmann I., Glowatzki H., Johnson R. L., Vollmer A., Rabe J. P., Koch N. *Nat. Mater.* **2008**, *7* (4), 326–332. https://doi.org/10.1038/nmat2119.

[9] Frischeisen J., Yokoyama D., Endo A., Adachi C., Brütting W. *Org. Electron.* **2011**, *12* (5), 809–817. https://doi.org/https://doi.org/10.1016/j.orgel.2011.02.005.

[10] Liehm P., Murawski C., Furno M., Lüssem B., Leo K., Gather M. C. *Appl. Phys. Lett.*

2012, *101* (25), 253304. https://doi.org/10.1063/1.4773188.

[11] Ediger M. D., de Pablo J., Yu L. *Acc. Chem. Res.* **2019**, *52* (2), 407–414.

https://doi.org/10.1021/acs.accounts.8b00513.

[12] Ediger M. D. *J. Chem. Phys.* **2017**, *147* (21), 210901.

https://doi.org/10.1063/1.5006265.

[13] Roscioni O. M., D'avino G., Muccioli L., Zannoni C. *J. Phys. Chem. Lett.* **2018**, *9* (23),

6900–6906. https://doi.org/10.1021/acs.jpclett.8b03063.

[14] Yokoyama D., Sakaguchi A., Suzuki M., Adachi C. *Appl. Phys. Lett.* **2008**, *93* (17).

https://doi.org/10.1063/1.2996258.

[15] Yokoyama D., Sakaguchi A., Suzuki M., Adachi C. *Org. Electron.* **2009**, *10* (1), 127–

137. https://doi.org/10.1016/j.orgel.2008.10.010.

[16] Sasabe H., Tanaka D., Yokoyama D., Chiba T., Pu Y.-J., Nakayama K., Yokoyama M.,

Kido J. *Adv. Funct. Mater.* **2011**, *21* (2), 336–342.

https://doi.org/10.1002/adfm.201001252.

[17] Yoo D., Song H., Youn Y., Jeon S. H., Cho Y., Han S. *Phys. Chem. Chem. Phys.* **2019**,

21 (3), 1484–1490. https://doi.org/10.1039/C8CP05294H.

[18] Youn Y., Yoo D., Song H., Kang Y., Kim K. Y., Jeon S. H., Cho Y., Chae K., Han S.

J. Mater. Chem. C **2018**, *6* (5), 1015–1022. https://doi.org/10.1039/C7TC05278B.

[19] Olivier Y., Sancho-Garcia J. C., Muccioli L., D'Avino G., Beljonne D. *J. Phys. Chem.*

Lett. **2018**, *9* (20), 6149–6163. https://doi.org/10.1021/acs.jpclett.8b02327.

[20] Hu T., Han G., Tu Z., Duan R., Yi Y. *J. Phys. Chem. C* **2018**, *122* (48), 27191–27197.

https://doi.org/10.1021/acs.jpcc.8b08169.

[21] Muccioli L., D'Avino G., Zannoni C. *Adv. Mater.* **2011**, *23* (39), 4532–4536.

https://doi.org/10.1002/adma.201101652.

[22] Walters D. M., Antony L., De Pablo J. J., Ediger M. D. *J. Phys. Chem. Lett.* **2017**, *8*

(14), 3380–3386. https://doi.org/10.1021/acs.jpclett.7b01097.

[23] Antony L. W., Jackson N. E., Lyubimov I., Vishwanath V., Ediger M. D., De Pablo J. J. *ACS Cent. Sci.* **2017**, *3* (5), 415–424. https://doi.org/10.1021/acscentsci.7b00041.

[24] Lee T., Caron B., Stroet M., M. Huang D., L. Burn P., E. Mark A. *Nano Lett.* **2017**, *17* (10), 6464–6468. https://doi.org/10.1021/acs.nanolett.7b03528.

[25] Tonnelé C., Stroet M., Caron B., Clulow A. J., Nagiri R. C. R., Malde A. K., Burn P. L., Gentle I. R., Mark A. E., Powell B. J. *Angew. Chemie - Int. Ed.* **2017**, *56* (29), 8402–8406. https://doi.org/10.1002/anie.201610727.

[26] Han G., Shen X., Yi Y. *Adv. Mater. Interfaces* **2015**, *2* (17), 1500329. https://doi.org/10.1002/admi.201500329.

[27] Berendsen H. J. C., Van Der Spoel D., Van Drunen R. *Comput. Phys. Commun.* **1995**, *91*, 43–56.

[28] Hess B., Kutzner C., van der Spoel D., Lindahl E. *J. Chem. Theory Comput.* **2008**, *4* (3), 435–447. https://doi.org/10.1021/ct700301q.

[29] Bussi G., Donadio D., Parrinello M. *J. Chem. Phys.* **2007**, *126*, 14101.

[30] Berendsen H. J. C., Postma J. P. M., van Gunsteren W. F., DiNola A., Haak J. R. *J. Chem. Phys.* **1984**, *81* (8), 3684–3690. https://doi.org/10.1063/1.448118.

[31] Hess B., Bekker H., Berendsen H. J. C., Fraaije J. G. E. M. *J. Comput. Chem.* **1997**, *18* (12), 1463–1472. https://doi.org/10.1002/(SICI)1096-987X(199709)18:12<1463::AID-JCC4>3.0.CO;2-H.

[32] Darden T., York D., Pedersen L. *J. Chem. Phys.* **1993**, *98* (12), 10089–10092. https://doi.org/10.1063/1.464397.

[33] Frisch M., Trucks G. W., Schlegel H. B., Scuseria G. E., Robb M. A., Cheeseman J. R., Scalmani G., Barone V., Mennucci B., Petersson G. A. ea. 2014.

[34] Chen B., Martin M. G., Siepmann J. I. *J. Phys. Chem. B* **1998**, *102* (14), 2578–2586. https://doi.org/10.1021/jp9801065.

[35] Dahlgren M. K., Schyman P., Tirado-Rives J., Jorgensen W. L. *J. Chem. Inf. Model.*

2013, *53* (5), 1191–1199. https://doi.org/10.1021/ci4001597.

[36] Jorgensen W. L., Mcdonald N. A. *Development of an All-Atom Force Field for Heterocycles. Properties of Liquid Pyridine and Diazenes'*; 1998; Vol. 424.

[37] Bernardes C. E. S., Joseph A. *J. Phys. Chem. A* **2015**, *119* (12), 3023–3034. https://doi.org/10.1021/jp512349r.

[38] Moral M., Son W.-J., Sancho-García J. C., Olivier Y., Muccioli L. *J. Chem. Theory Comput.* **2015**, *11* (7), 3383–3392. https://doi.org/10.1021/acs.jctc.5b00164.

[39] Marcus R. A. *Advances in Chemical Physics*. January 1, 1999, pp 1–6. https://doi.org/doi:10.1002/9780470141656.ch1.

[40] D'Avino G., Muccioli L., Castet F., Poelking C., Andrienko D., Soos Z. G., Cornil J., Beljonne D. *J. Phys. Condens. Matter* **2016**, *28* (43). https://doi.org/10.1088/0953-8984/28/43/433002.

[41] D'Avino G., Muccioli L., Zannoni C., Beljonne D., Soos Z. G. *J. Chem. Theory Comput.* **2014**, *10* (11), 4959–4971. https://doi.org/10.1021/ct500618w.

[42] D'Avino G., Duhm S., Della Valle R. G., Heimel G., Oehzelt M., Kera S., Ueno N., Beljonne D., Salzmann I. *Chem. Mater.* **2020**, *32* (3), 1261–1271. https://doi.org/10.1021/acs.chemmater.9b04763.

[43] Gali S. M., D'Avino G., Aurel P., Han G., Yi Y., Papadopoulos T. A., Coropceanu V., Brédas J.-L., Hadziioannou G., Zannoni C., Muccioli L. *J. Chem. Phys.* **2017**, *147* (13), 134904. https://doi.org/10.1063/1.4996969.

[44] Frisch M. J., Trucks G. W., Schlegel H. B., Scuseria G. E., Robb M. a., Cheeseman J. R., Scalmani G., Barone V., Petersson G. a., Nakatsuji H., Li X., Caricato M., Marenich a. V., Bloino J., Janesko B. G., Gomperts R., Mennucci B., Hratchian H. P., Ortiz J. V., Izmaylov a. F., Sonnenberg J. L., Williams, Ding F., Lipparini F., Egidi F., Goings J., Peng B., Petrone A., Henderson T., Ranasinghe D., Zakrzewski V. G., Gao J., Rega N., Zheng G., Liang W., Hada M., Ehara M., Toyota K., Fukuda R., Hasegawa

J., Ishida M., Nakajima T., Honda Y., Kitao O., Nakai H., Vreven T., Throssell K.,

Montgomery Jr. J. a., Peralta J. E., Ogliaro F., Bearpark M. J., Heyd J. J., Brothers E.

N., Kudin K. N., Staroverov V. N., Keith T. a., Kobayashi R., Normand J.,

Raghavachari K., Rendell a. P., Burant J. C., Iyengar S. S., Tomasi J., Cossi M.,

Millam J. M., Klene M., Adamo C., Cammi R., Ochterski J. W., Martin R. L.,

Morokuma K., Farkas O., Foresman J. B., Fox D. J. 2016.

[45] Neese F. *WIREs Comput. Mol. Sci.* **2012**, *2* (1), 73–78.

https://doi.org/10.1002/wcms.81.

[46] Senthilkumar K., Grozema F. C., Bickelhaupt F. M., Siebbeles L. D. A. *J. Chem. Phys.*
2003, *119* (18), 9809–9817. https://doi.org/10.1063/1.1615476.

[47] López-Estrada O., Laguna H. G., Barrueta-Flores C., Amador-Bedolla C. *ACS Omega*
2018, *3* (2), 2130–2140. https://doi.org/10.1021/acsomega.7b01425.

[48] Tummala N. R., Zheng Z., Aziz S. G., Coropceanu V., Brédas J.-L. *J. Phys. Chem.
Lett.* **2015**, *6* (18), 3657–3662. https://doi.org/10.1021/acs.jpclett.5b01709.

[49] Faber C., Janssen J. L., Côté M., Runge E., Blase X. *Phys. Rev. B* **2011**, *84* (15),
155104. https://doi.org/10.1103/PhysRevB.84.155104.

[50] Le Roux S., Petkov V. *J. Appl. Crystallogr.* **2010**, *43* (1), 181–185.

https://doi.org/10.1107/S0021889809051929.

[51] Yokoyama D. *J. Mater. Chem.* **2011**, *21* (48), 19187–19202.

https://doi.org/10.1039/c1jm13417e.

[52] Ziener U., Lehn J.-M., Mourran A., Möller M. *Chem. – A Eur. J.* **2002**, *8* (4), 951–957.

https://doi.org/10.1002/1521-3765(20020215)8:4<951::AID-CHEM951>3.0.CO;2-9.

[53] Meier C., Ziener U., Landfester K., Weihrich P. *J. Phys. Chem. B* **2005**, *109* (44),
21015–21027. https://doi.org/10.1021/jp054271d.

[54] Ziener U. *J. Phys. Chem. B* **2008**, *112* (47), 14698–14717.

https://doi.org/10.1021/jp805846d.

[55]   Meier C., Landfester K., Ziener U. *J. Phys. Chem. C* **2009**, *113* (4), 1507–1514.

https://doi.org/10.1021/jp808431t.

[56]   Meier C., Roos M., Künzel D., Breitruck A., E. Hoster H., Landfester K., Gross A.,

Jürgen Behm R., Ziener U. *J. Phys. Chem. C* **2009**, *114* (2), 1268–1277.

https://doi.org/10.1021/jp910029z.

[57]   van der Spoel D., J. van Maaren P., Larsson P., Tîmneanu N. *J. Phys. Chem. B* **2006**,

110 (9), 4393–4398. https://doi.org/10.1021/jp0572535.

[58]   Bin Z., Liu Z., Qiu Y., Duan L. *Adv. Opt. Mater.* **2018**, *6* (18), 1800536.

https://doi.org/10.1002/adom.201800536.

[59]   Bässler H. *Phys. status solidi* **1993**, *175* (1), 15–56.

https://doi.org/10.1002/pssb.2221750102.

Antonio De Nicola,* Andrea Correa, Andrea Giunchi, Luca Muccioli, Gabriele D'Avino, Junji Kido and Giuseppe Milano

Bidimensional H-Bond Network Promoters Structural Order and Electron Transport in BPyMPMs Molecular Semiconductor
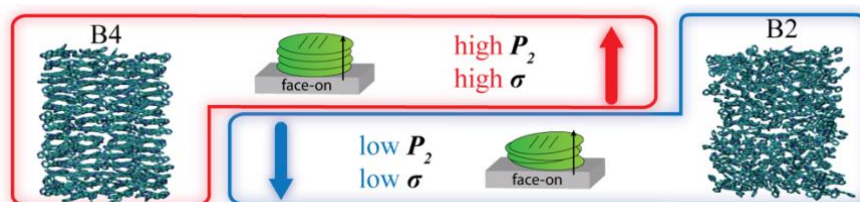
Surprisingly higher electron mobility in the thin film of B4PyMPM (B4), two orders of magnitude higher than mobility measured for other components of the BPyMPM family is experimentally found. The present computational study elucidates the molecular origin of that difference, arising in the higher hydrogen bonds formed by B4, which promote a higher orientational order P2 and electron transport properties.